PHYSICAL REVIEW B **74**, 125117 (2006)

Doped AB_2 Hubbard chain: Spiral, Nagaoka and resonating-valence-bond states, phase separation, and Luttinger-liquid behavior

R. R. Montenegro-Filho and M. D. Coutinho-Filho
Laboratório de Física Teórica e Computacional, Departamento de Física, Universidade Federal de Pernambuco,
50670-901 Recife-PE, Brazil

(Received 12 May 2006; revised manuscript received 31 July 2006; published 28 September 2006)

We present an extensive numerical study of the Hubbard model on the doped AB_2 chain, both in the weak coupling and the infinite-U limit. Due to the special unit-cell topology, this system displays a rich variety of phases as a function of hole doping (δ) away from half-filling. Near half-filling spiral states develop in the weak-coupling regime, while Nagaoka itinerant ferromagnetism is observed in the infinite-U limit. For higher doping, the system phase-separates before reaching a Mott insulating phase of short-range resonating-valence-bond states at $\delta=1/3$. Moreover, for $\delta>1/3$ we observe a crossover, which anticipates the Luttinger-liquid behavior for $\delta>2/3$.

DOI: 10.1103/PhysRevB.74.125117 PACS number(s): 71.10.Fd, 74.20.Mn, 75.30.Kz

I. INTRODUCTION

Low-dimensional strongly correlated electron systems have attracted a great deal of attention in the past two decades. The reason dates back to Anderson's proposal[1] that the t-J version of the Hubbard model might carry the basic mechanisms underlying the high-T_c superconductivity observed in CuO_2 compounds. Despite the fact that this remains an open issue, the above suggestion fertilized intensive investigations on many related fundamental topics, such us itinerant electron magnetism, Mott metal-insulator transitions, and quantum critical phenomena. Among several features of interest, we mention the possibility of the realization of spiral,[2] Nagaoka,[3–5] and resonating-valence-bond (RVB) states,[6] spatially separated phases,[7,8] and Luttinger-liquid behavior,[9] which may present strong deviations from the Landau Fermi liquid theory.

In this work, we report numerical results of the Hubbard model on the doped AB_2 chain away from half-filling, which show that its special unit-cell topology greatly enriches the phase diagram found in the doped standard linear chain. In fact, all features mentioned above are shown to be associated with well defined ground-state (GS) phases of this doped chain. Doped AB_2-Hubbard chains were previously studied through Hartree-Fock, quantum Monte Carlo, and exact diagonalization (ED) techniques both in the weak- and strong-coupling limits,[10] including also the t-J model[11] using the density-matrix renormalization group (DMRG) and recurrent variational *Ansätzes*, and the infinite-U limit[12] using ED. In particular, these chains represent an alternative route to reaching two-dimensional quantum physics from one-dimensional systems.[11,13] At half-filling, the AB_2-Hubbard chain exhibits a quantum ferrimagnetic GS,[10,14–16] whose magnetic excitations have been studied in detail both in the weak- and strong-coupling limits,[17] and in the light of the quantum Heisenberg model.[17,18] Further studies have considered the anisotropic[19] and isotropic[20] critical behavior of the AB_2-quantum-Heisenberg model, including its spherical version,[21] and the statistical mechanics of the AB_2-classical-Heisenberg model.[22]

On the experimental side, the AB_2 chain topology is of relevance to the understanding of the physics of some low-dimensional strongly correlated electronic systems. One class is the line of trimer clusters present in phosphates with formula $A_3Cu_3(PO_4)_4$, where A=Ca,[23–26] Sr,[24–27] and Pb.[25,26,28] The trimers have three Cu^{2+} ($S=1/2$) paramagnetic ions antiferromagnetically coupled. Although the superexchange intertrimer interaction is much weaker than the intratrimer coupling, it proves sufficient to turn them into bulk ferrimagnets. Another quasi-one-dimensional inorganic material closely associated with the ferrimagnetic phase of the AB_2 chain is the NiCu bimetallic chain.[29] These compounds display alternating Ni^{2+} ($S=1$) and Cu^{2+} ($S=1/2$) ions connected through suitable ligands in a line, and are modeled by the alternating spin-$\frac{1}{2}$/spin-1 antiferromagnetic Heisenberg chain.[30] We would also like to mention a more recently synthesized organic ferrimagnetic compound consisting of three $S=1/2$ paramagnetic radicals[31] in its magnetic unit cell, as well as possible connections with the physics of the oxocuprates.[32]

This paper is organized as follows. In Sec. II, we introduce the model system and the numerical techniques used to calculate several quantities suitable to characterize the occurrence of distinct phases as a function of doping and Coulomb coupling. In Sec. III, we discuss spiral and Nagaoka states at low hole doping, whose magnetic properties are shown to exhibit very interesting features in the weak and infinite-U limit, respectively. In Sec. IV, we show that for higher hole doping the system phase-separates, before reaching a Mott insulating phase of short-range RVB states at $\delta=1/3$. In Sec. V, we discuss several features of the crossover region, which takes place before the Luttinger-liquid behavior observed for $\delta>2/3$. Finally, in Sec. VI we present a summary and some conclusions concerning the reported results.

II. MODEL DESCRIPTION AND METHODS

The AB_2 chain is a bipartite lattice with three sites (named A, B_1, and B_2) per unit cell, as illustrated in Fig. 1(a). The Hubbard Hamiltonian for a lattice with N_c unit cells and N sites reads

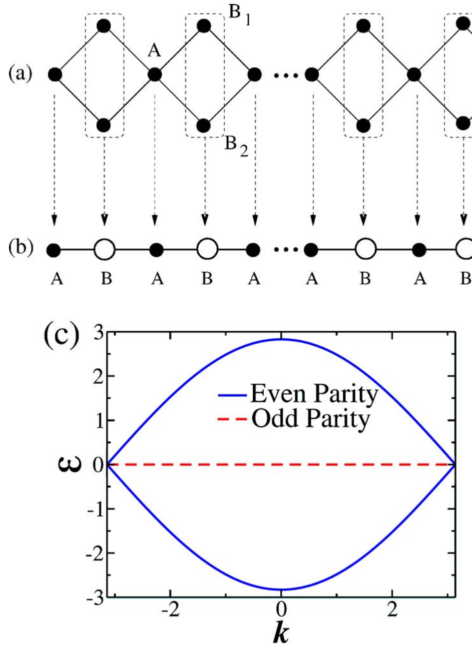

FIG. 1. (Color online) (a) Illustration of the AB_2 chain showing A, B_1, and B_2 sites. (b) Illustration of the effective linear chain (ELC). (c) Electronic bands of the tight-binding model: two dispersive (continuous line) and one flat (dashed line).

$$H = -t\sqrt{2}\sum_{l=1,\sigma}^{N_c}[b_{l\sigma}^{\dagger}(A_{l\sigma}+A_{l+1,\sigma})+\text{H.c.}]+U\sum_{i=1}^{N}n_{i\uparrow}n_{i\downarrow}, \quad (1)$$

where $A_{l\sigma}^{\dagger}$ and $b_{l\sigma}^{\dagger}=\frac{1}{\sqrt{2}}(B_{1,l\sigma}^{\dagger}+B_{2,l\sigma}^{\dagger})$ are the creation operators of an electron with spin σ at site A and in a bonding state between sites B_1 and B_2 of the cell l, respectively, $t(\equiv 1)$ is the hopping amplitude, and U is the Coulomb coupling. For $U=\infty$, double occupancy is completely excluded and the Hamiltonian takes the form

$$H = -t\sqrt{2}\sum_{l=1,\sigma}^{N_c}P_G[b_{l\sigma}^{\dagger}(A_{l\sigma}+A_{l+1,\sigma})+\text{H.c.}]P_G, \quad (2)$$

where $P_G=\Pi_i(1-n_{i\uparrow}n_{i\downarrow})$ is the Gutzwiller projector operator. The model is invariant under the interchange of the B sites of the same cell, a symmetry that implies a well-defined local parity ($p_l=\pm 1$) for the GS wave function. As a result, in computing some quantities, we find it convenient to use the effective linear chain (ELC) generated by the map illustrated in Figs. 1(a) and 1(b), i.e., any quantity $X_{B,l}$ associated with a B site at cell l of the ELC is given by $X_{B_1,l}+X_{B_2,l}$. This mapping does not change the physical content of the GS and excited states, being used only to expose in a more clear fashion some properties of these states.

In the tight-binding description ($U=0$), this model presents three bands:[10] one flat with N_c odd-parity states [antibonding orbitals, $a_{l\sigma}^{\dagger}=\frac{1}{\sqrt{2}}(B_{1,l\sigma}^{\dagger}-B_{2,l\sigma}^{\dagger})$] and energy $\epsilon=0$, and two dispersive branches,

$$\epsilon_{\pm}(k) = \pm 2\sqrt{2}\cos(k/2), \quad (3)$$

with $k=2\pi l/N_c$, $l=0,1,2,\ldots,N_c-1$, built from A sites and bonding (even-parity) orbitals, as shown in Fig. 1(c). At half-filling ($N_e=N$, where N_e is the number of electrons), the GS total spin S_g is degenerate, with S_g ranging from the minimum value (0 or 1/2) to $S_g=|N_B-N_A|/2$, where N_A (N_B) is the number of sites in the A (B) sublattice. As proved by Lieb,[33] the Coulomb repulsion lifts this huge degeneracy and selects the

$$S_g = |N_B - N_A|/2 \equiv S_{\text{Lieb}} \quad (4)$$

ground state for any finite U, giving rise to a ferrimagnetic GS.[10,14,17]

On the other hand, for $U=\infty$, one hole ($N_e=N-1$), and periodic boundary conditions (BC's), the system satisfies the requirements of Nagaoka's theorem for saturated ferromagnetism.[10,12] For Nagaoka ferromagnetism and Lieb ferrimagnetism, the GS is homogeneous in parity with $p_l=-1$ for any cell l. Due to this symmetry, the spectrum of the AB_2 chain in the Heisenberg limit ($U\gg t$, $N_e=N$) at the sector $p=-1$ [see Eq. (5)] is identical to that of the alternating Heisenberg spin-$\frac{1}{2}$/spin-1 chain.[30]

Here we focus on the effect of hole doping, $\delta=1-(N_e/N)$, both in the weak coupling and the infinite-U limit, using exact diagonalization (ED) through the Lanczos algorithm for closed BC's and DMRG for open BC's.[34] In the ED procedure, the BC's are such that they minimize the energy, except for $U=2$ and $\delta\leq 1/3$ [Fig. 2(c)], in which the BC's (periodic or antiperiodic) are such that the Fermi wave vector k_F in the thermodynamic limit is included in the set of wave vectors for the finite system.[35] We used finite-size DMRG for open chains with A sites in its extrema, keeping 364 to 546 states per block in the last sweep. The maximum discarded weight in the last sweep was typically $\sim 10^{-7}$, except for odd phases and $U=2$, where the discarded weight was $\sim 10^{-5}$. In the DMRG calculations, we treated B_1 and B_2 as a composite site with nine states for $U=\infty$ and 16 states for $U=2$. However, by considering the parity symmetry, we can decompose this supersite into the two possible symmetry sectors +1 and −1. Within this scheme, we have considered all parity symmetry sectors of the form $(-)^x(+)^{N_c-x}$, with x contiguous cells of odd parity in one side of the open chain and N_c-x contiguous cells of even parity in the other. In addition, we have verified the stability of this phase separation against the formation of a mixed phase composed of smaller domains. The energy is studied as a function of x for an increasing number of states kept per block in order to localize the value of x for which the energy is minimum, as shown in Figs. 2(a) and 2(b). The phase-separated boundaries are thus determined by the limiting dopings for which an inhomogeneous phase (nonuniform parities) is observed. We have also developed a simple variational approach for $U=\infty$ and $\delta\leq 1/3$, which is explained in detail in the Appendix. The results calculated using this approach are shown in Figs. 2(d) and 3(c).

In Fig. 2(c) ($U=2$) and Fig. 2(d) ($U=\infty$), we present the average parity,

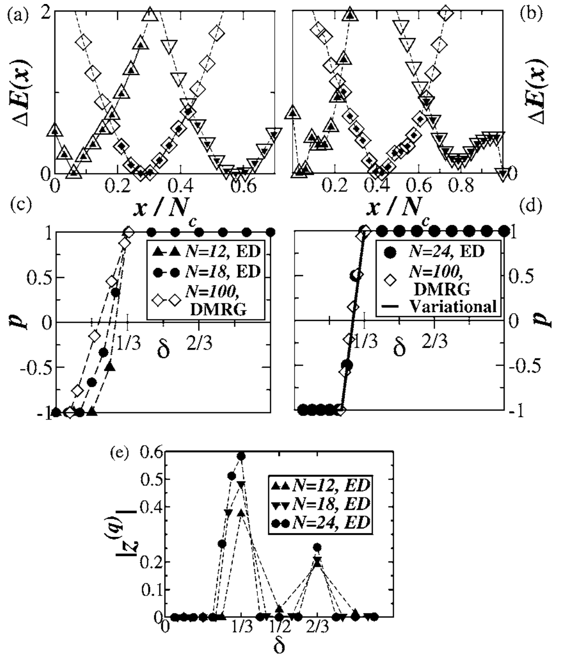

FIG. 2. DMRG results for the energy difference between the lowest energy at the symmetry sector $(-)^x(+)^{N_c-x}$ and the GS energy for $N=100$ ($N_c=33$) for (a) $U=2$ at $\delta=0.32$ (triangle up), $\delta=0.26$ (diamond), and $\delta=0.18$ (triangle down); (b) $U=\infty$ at $\delta=0.32$ (triangle up), $\delta=0.28$ (triangle up), and $\delta=0.24$ (triangle down), taking 108 states per block (open symbols) and 216 states per block (filled symbols). Average local parity p as a function of δ for (c) $U=2$ and (d) $U=\infty$. (e) ED results for $|z^{(q)}|$. Dashed lines are guides to the eye.

$$p \equiv \frac{1}{N_c}\sum_{l=1}^{N_c} p_l, \qquad (5)$$

as a function of doping, computed using the above-mentioned methods. In both regimes, we observe the occurrence of a homogeneous phase near half-filling with $p=-1$. For higher doping, i.e., $\delta_{\mathrm{PS}}(U)<\delta<(1/3)$ [$\delta_{\mathrm{PS}}(2)\approx 0.07$ and $\delta_{\mathrm{PS}}(\infty)\approx 0.22$], the system phase-separates in one region with odd-parity cells and the other with even ones. For $\delta \geq 1/3$, the GS is homogeneous with $p=1$.

In order to present an overview of the conducting properties of the AB_2 chain phases in the infinite-U limit, we display in Fig. 2(e) the quantity[36]

$$|z^{(q)}| = \left|\left\langle \exp\left(\frac{2\pi q i}{L}\sum_j x_j\right)\right\rangle\right|, \qquad (6)$$

calculated in the ELC using ED, where $L=2N_c$, $x_j=jn_j$, n_j is the electron density at site j, and q is such that $\frac{N_e}{L}=\frac{p}{q}$, with p and q coprimes. The phase of $z^{(q)}$ corresponds to the GS expectation value of the position operator, while its modulus defines the localization length; in an insulator, $|z^{(q)}|\to 1$ as $L\to\infty$, while in a conductor, $|z^{(q)}|\to 0$ for closed boundary conditions.[36] The increase of $|z^{(q)}|$ with system size for $\delta=2/3$ and $1/3$, as well as in the phase-separated region, is evidence of insulating phases at these dopings. These conclusions will be better confirmed by studying the Drude weight using ED and the charge gap for larger systems with DMRG.

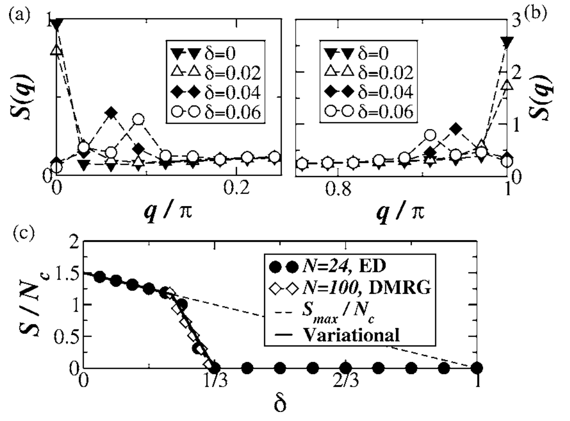

FIG. 3. (a) and (b) Magnetic structure factor for $U=2$ and $N=100$ in the underdoped region. (c) Total spin per cell S/N_c as function of δ for $U=\infty$.

III. SPIRAL STATES AND SATURATED FERROMAGNETISM

In Figs. 3(a) and 3(b), we display the magnetic structure factor

$$S(q) = \frac{1}{S_{\mathrm{Lieb}}(S_{\mathrm{Lieb}}+1)}\sum_{l,m}^{2N_c+1} e^{iq(l-m)}\langle \mathbf{S}_l \cdot \mathbf{S}_m\rangle, \qquad (7)$$

calculated at $S^z=0$ and $U=2$ using DMRG for the ELC. First, notice the presence of peaks at $q=0$ and $q=\pi$ revealing the ferrimagnetic order at half-filling. These peaks sustain up to two holes ($\delta=0.02$); however, it is not clear whether the ferrimagnetic phase is robust against doping in the thermodynamic limit. Indeed, by increasing the hole doping, spiral peaks at δ-dependent positions appear near $q=0$ and $q=\pi$. The analysis of the charge gap,

$$\Delta_c = E(N_e+1) + E(N_e-1) - 2E(N_e), \qquad (8)$$

suggests that these states are metallic, in opposition to the Mott insulating ferrimagnetic state at $\delta=0$. It is worth mentioning that the occurrence of spiral phases in oxocuprates has been a challenging and topical subject.[32]

In Fig. 3(c), we present the GS total spin as a function of doping for $U=\infty$. For $\delta<\delta_{\mathrm{PS}}(\infty)$, itinerant saturated ferromagnetism due to hole kinematics (Nagaoka mechanism) is observed. It is interesting to notice that our estimate for the upper hole density ($\gtrsim 0.2$) beyond which Nagaoka ferromagnetism is unstable is in very good agreement with similar predictions for ladders[37,38] and the square lattice.[39]

We have also considered the presence of an Aharonov-Bohm flux Φ for a closed chain through the gauge transformation,

$$b_{l\sigma} \to b_{l\sigma}e^{2\pi i\Phi l/N_c}, \quad A_{l\sigma} \to A_{l\sigma}e^{2\pi i\Phi l/N_c}, \qquad (9)$$

with $\Phi_0=hc/e\equiv 1$. The flux variation is equivalent to a change in the boundary condition: $\Phi=0$ represents periodic

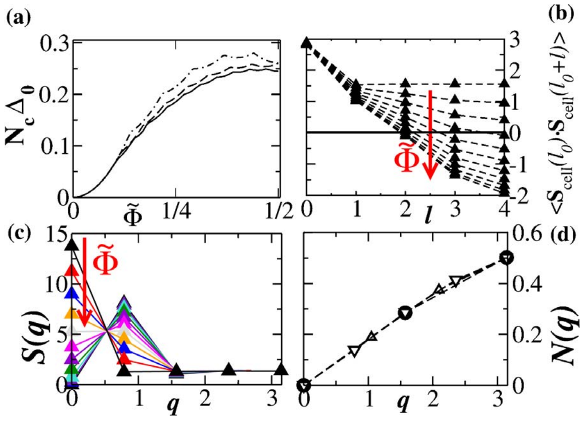

FIG. 4. (Color online) ED results of (a) N_c times the energy gap Δ_0 between the saturated ferromagnetism energy ($\Phi=\Phi_F$) and the lowest energy state for an Aharanov-Bohm flux Φ as a function of $\tilde{\Phi}=|\Phi-\Phi_F|$ at $\delta=1/6$ and $N_c=4$ (dashed-dot line), 6 (dashed line), and 8 (solid line). ED calculation for the $\tilde{\Phi}$-dependent behavior of (b) the spin correlation function $\langle \mathbf{S}_{\text{cell}}(l_0)\cdot\mathbf{S}_{\text{cell}}(l_0+l)\rangle$ between the cell spins as a function of l and (c) the magnetic structure factor as a function of lattice wave vector q at $\delta=1/6$. (d) Charge structure factor calculated at the lowest-energy state for any $\tilde{\Phi}$ at $\delta=1/6$ for $N_c=4$ (●), 6 (▲), and 8 (▽).

and $\Phi=1/2$ antiperiodic boundary conditions. In Fig. 4(a), we present the dependence of the energy gap Δ_0 between the lowest-energy state for a flux Φ and that for saturated ferromagnetism ($\Phi\equiv\Phi_F$) as a function of $\tilde{\Phi}=|\Phi-\Phi_F|$ at $\delta=1/6$. We have identified many level crossings in this curve. In fact, as the flux increases from Φ_F, the total spin decreases from the maximum value, $S=N_e/2$, to the minimum value, $S=0$ ($S=1/2$), for N_e even (odd), a behavior also observed in the square lattice.[40] Notice that $N_c\Delta_0$ tends to saturation with system size, indicating that the level spacings decrease with $1/N_c$. These results suggest that the thermodynamic GS displays spontaneously SU(2) symmetry breaking as a result of an ergodic combination of infinitely many states ($N_c\to\infty$), including the singlet spiral state.[41] In Figs. 4(b) and 4(c) we present the spin correlation function between cell spins $\mathbf{S}_{\text{cell}}(l)=\mathbf{S}_A(l)+\mathbf{S}_{B_1}(l)+\mathbf{S}_{B_2}(l)$ and the magnetic structure factor

$$S(q)=\frac{1}{N_c}\sum_{\langle l,m\rangle} e^{iq(l-m)}\langle \mathbf{S}_{\text{cell}}(l)\cdot\mathbf{S}_{\text{cell}}(m)\rangle \tag{10}$$

as a function of distance l and wave vector $q=2\pi l/N_c$, $l=0,\ldots,N_c$, respectively. As we can observe, the saturated ferromagnetic and the spiral singlet states are adiabatically connected, such that all states contributing to the thermodynamic GS exhibit long-range ordering. In particular, as the flux increases from Φ_F, the peak of $S(q)$ at $q=0$ (saturated ferromagnetism) steadily decreases, while the spiral state peak at $q=2\pi/N_c$ increases. We noted also that the charge structure factor

$$N(q)=\frac{1}{N_c}\sum_{\langle l,m\rangle} e^{iq(l-m)}\langle \Delta n_l \Delta n_m\rangle, \tag{11}$$

where $\Delta n_l=n_l-\langle n_l\rangle$ and n_l is the electron occupation number at cell l, is not affected by the flux variation and displays a peak at $2k_F=\pi$ [Fig. 4(d)], where k_F is the tight-binding *spinless* Fermi wave vector,[10] with $k_F=3\pi\delta$, $\delta\leq 1/3$.

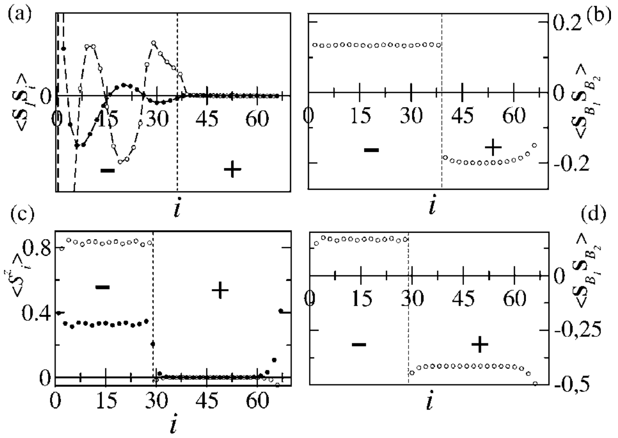

FIG. 5. GS properties at $\delta=0.18$ ($U=2$) and $\delta=0.28$ ($U=\infty$) for $N=100$ using DMRG. (a) Spin correlation function $\langle \mathbf{S}_1\cdot\mathbf{S}_i\rangle$ for $U=2$. (b) Expectation value of S_i^z for $U=\infty$ in the sector $S^z=S_g$. Spin correlation function $\langle \mathbf{S}_{B_1}\cdot\mathbf{S}_{B_2}\rangle_i$ for (c) $U=2$ and (d) $U=\infty$. − (+) indicates odd (even) local parity. Effective linear chain notation: (●) identifies A sites and (○) B_1+B_2 at the same cell. Dashed lines are guides to the eye.

IV. PHASE SEPARATION AND RVB STATES

In the phase-separated regime, the charge compressibility diverges following the linear dependence of the energy with doping. In Figs. 5 and 6, we present some properties of the GS in this regime calculated through DMRG for the ELC. First we notice that all these properties clearly exhibit some

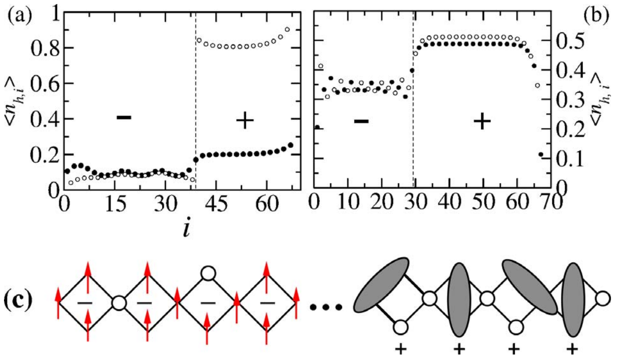

FIG. 6. (Color online) GS properties at $\delta=0.18$ ($U=2$) and $\delta=0.28$ ($U=\infty$) for $N=100$ using DMRG. Expectation value of $n_{h,i}$ for (a) $U=2$ and (b) $U=\infty$. Effective linear chain notation: (●) identifies A sites and (○) B_1+B_2 at the same cell. (c) Illustration of the GS for $U=\infty$ in the phase-separated regime: singlet bonds are represented by ellipses and holes by circles. − (+) indicates odd (even) local parity. Dashed lines are guides to the eye.

modulation on the same sublattice in the *metallic* odd-parity region due to charge itinerancy. In particular, this modulation is stronger in the $U=2$ spiral phase as evidenced by the correlation function $\langle \mathbf{S}_1\cdot\mathbf{S}_i\rangle$ shown in Fig. 5(a), but also noticed in the itinerant Nagaoka phase ($U=\infty$) as manifested by the site magnetization $\langle S_i^z\rangle$ shown in Fig. 5(c). On the other hand, in the *insulating* even-parity phase, a flat behavior is observed, except for boundary and interface effects. These paramagnetic phases [see Figs. 5(b) and 5(d)] are characterized by strong singlet correlations between spins at sites B_1 and B_2 at the same cell, i.e., $\langle \mathbf{S}_{B_1}\cdot\mathbf{S}_{B_2}\rangle\approx-0.20$ (≈-0.41) for $U=2$ ($=\infty$), as shown in Figs. 5(b) and 5(d). In contrast, in the metallic phase this correlation varies very little with U and indicates robust triplet correlations, i.e., $\langle \mathbf{S}_{B_1}\cdot\mathbf{S}_{B_2}\rangle\approx0.13$ (≈0.16) for $U=2$ ($=\infty$). Notice that in the absence of hole hopping, even when restricted to a cell as in the insulating phase, the value of $\langle \mathbf{S}_{B_1}\cdot\mathbf{S}_{B_2}\rangle$ in a singlet (triplet) state should be -0.75 (0.25). The hole density $\langle n_{h,i}\rangle$ is shown in Figs. 6(a) and 6(b). In the odd-parity metallic phase, holes do not occupy antibonding orbitals, whereas in the even-parity insulating phase these orbitals are accessible for them. Therefore, in the first case the hole densities at sites A and B_1+B_2 are very similar. This may also occur in the second case if double occupancy is excluded ($U=\infty$). An illustration of the phase-separated regime for $U=\infty$ is shown in Fig. 6(c). In this coupling limit, unsaturated ferromagnetism was suggested to occur in ladders[37] and the square lattice[39] as an intermediate phase between saturated ferromagnetism and paramagnetism as a function of doping. However, in the context of the t-J model, the situation is more complex and predictions of phase separation, both for ladders[38] and the square lattice,[7,42,43] and stripe formation for the square lattice[42] have been reported.

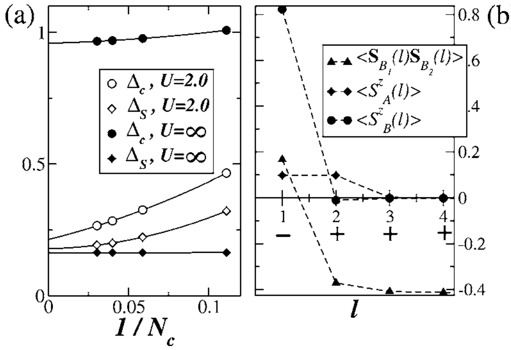

FIG. 7. DMRG results for (a) the size dependence of the charge (Δ_c) and spin (Δ_S) gaps as a function of $1/N_c$ at $\delta=1/3$: solid lines are polynomial fittings. ED results for (b) the expectation values of $S_A^z(l)$, $S_B^z(l)$ and the correlation function $\langle \mathbf{S}_{B_1}(l)\cdot\mathbf{S}_{B_2}(l)\rangle$ at spin sector $S^z=1$ as a function of cell number l. The ± signs below the horizontal axis in (b) indicate the cell parity.

At $\delta=1/3$, i.e., one hole per A site for open BC's using DMRG,[11] the GS has even parity and is fully dominated by the Mott insulating phase (even parity) illustrated in Fig. 6(c) for $U=\infty$. The charge gap $\Delta_c=\mu_+-\mu_-$, where $\mu_+=[E(N_e+\Delta N_e)-E(N_e)]/\Delta N_e$, $\Delta N_e>0$ ($\Delta N_e/N\to0$), and $\mu_-=E(N_e)-E(N_e-1)$, must be calculated with care. First, notice that adding electrons to $\delta=1/3$ places the system in the phase-separated (inhomogeneous) region where the chemical potential μ is flat. Indeed, by comparing results using DMRG and ED calculations, for $U=\infty$, for which Δ_c presents little finite-size corrections [Fig. 7(a)], we concluded that boundary effects are minimized by taking $\Delta N_e=2$ and placing the symmetry inverted cells at the chain center. We thus find [Fig. 7(a)] $\Delta_c\approx0.21$ (≈0.96) for $U=2$ ($=\infty$). This problem is absent in the case of hole doping since the phase is homogeneous. The extrapolated spin gap,

$$\Delta_S=E(S=1)-E(S=0), \tag{12}$$

characterized by symmetry inversion of a cell at the chain center, is also shown in Fig. 7(a) for $U=2$ ($\Delta_S\approx0.18$) and $U=\infty$ ($\Delta_S\approx0.16$), with the spin gap at $U=\infty$ presenting little finite-size dependence. It is quite a massive excitation with the magnetic exciton localized at the odd symmetry cell, mostly at the B sites, as shown in Fig. 7(b). In this context, Sierra *et al.*[11] found $\Delta_S\approx0.27$ using the t-J model ($J=4t^2/U$) for $J=0.35t$, i.e., $U\approx11.43$. We have confirmed this result by studying the U dependence of Δ_S using ED. In Fig. 8, we show that the spin correlation functions at $\delta=1/3$, calculated using DMRG, present a fast decay and can be fitted with the exponential form $\exp[-(l-l_c)/\xi]$, where ξ is the correlation length, l is the cell index in the ELC, and l_c denotes the central cell of the system. This behavior is expected from the presence of a finite spin gap. The values of ξ for the correlations $\langle \mathbf{S}_A(l_c)\cdot\mathbf{S}_A(l)\rangle$, $\langle \mathbf{S}_A(l_c)\cdot\mathbf{S}_B(l)\rangle$, and $\langle \mathbf{S}_B(l_c)\cdot\mathbf{S}_B(l)\rangle$ are ≈0.4 (2.2), 0.25 (0.45), and 0.39 (0.75), respectively, for $U=\infty$ ($U=2$), with l_c denoting the central

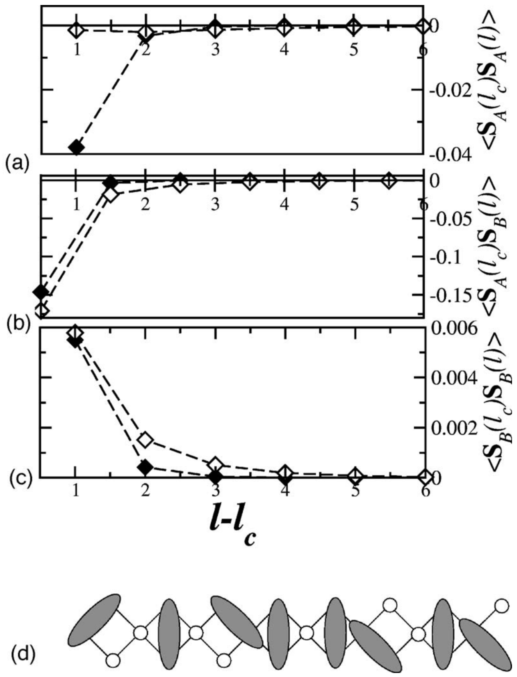

FIG. 8. Spin correlation functions (a) $\langle \mathbf{S}_A(l_c)\cdot\mathbf{S}_A(l)\rangle$, (b) $\langle \mathbf{S}_A(l_c)\cdot\mathbf{S}_B(l)\rangle$, and (c) $\langle \mathbf{S}_B(l_c)\cdot\mathbf{S}_B(l)\rangle$ as a function of $l-l_c$ in the ELC at $\delta=1/3$ for $N_c=33$ using DMRG; in the above expressions, l_c denotes the central cell; (◇) refers to $U=2$ and (◆) to $U=\infty$. Dashed lines are guides to the eye. (d) Illustration of the GS at $\delta=1/3$; singlet bonds are represented by ellipses and holes by circles.

cell. Thus, except for the correlation $\langle \mathbf{S}_A(l_c)\cdot\mathbf{S}_A(l)\rangle$ at $U=2$, the correlation length is extremely short with spins correlated only within a cell. Further, the calculated bulk values of $\langle \mathbf{S}_{B_1}\cdot\mathbf{S}_{B_2}\rangle$ at $\delta=1/3$ are in very good agreement with those in the even phase of the separated region shown in Figs. 5(b) and 5(d). The above results support a short-range-RVB (SR-RVB)[44] state for the GS at $\delta=1/3$, as illustrated in Fig. 8(d). In this context, Sierra *et al.*[11] reached similar conclusions using the *t*-*J* model on the AB_2 chain, while Giesekus has proved[45] that a SR-RVB state is the GS of a nonbipartite lattice with the same local symmetry but a different hopping pattern.

V. LUTTINGER-LIQUID BEHAVIOR

We now focus on the behavior of the system for $1/3<\delta<1$ by considering a chain with closed boundary conditions and $N_c=8$ for $U=\infty$ using ED. The first noticeable feature is the behavior of the spin correlation functions after doping the $\delta=1/3$ GS with two holes. The value of $\langle \mathbf{S}_{B_1}(l_0)\cdot\mathbf{S}_{B_2}(l_0)\rangle$ (where l_0 denotes an arbitrary cell) changes from -0.41 to -0.28. This variation can be understood by considering that the two holes added to the system break two singlet bonds and reside predominately at B sites. In this picture, the correlation function would amount to $\frac{N_c-2}{N_c}(-0.41)\approx-0.31$, which is close to -0.28. Furthermore, the spin correlation functions shown in Fig. 9(a) evidence the formation of long-ranged bonds between electrons on B sites, while the other correlations remain short-ranged, as in the $\delta=1/3$ ground state. This fact indicates that the electrons picked from the SR-RVB by hole doping are antiferromagnetically coupled and delocalized through the system, as illustrated in Fig. 9(b). In order to describe the system behavior for finite dopings, we display in Fig. 9(c) the correlation function $\langle \mathbf{S}_{B_1}(l_0)\cdot\mathbf{S}_{B_2}(l_0)\rangle$ and electronic densities as a function of δ. Notice that for $1/3<\delta<2/3$, the electronic density at A sites is almost fixed, while that at B sites is monotonically depopulated. As a consequence, $\langle \mathbf{S}_{B_1}(l_0)\cdot\mathbf{S}_{B_2}(l_0)\rangle$ continuously vanishes as the doping increases. Moreover, in Fig. 9(d) we show the relevant nearest-neighbor spin correlation functions. These correlations display quite different magnitudes at $\delta=1/3$, but their values approach each other for $\delta>2/3$. We thus consider the doping interval $1/3<\delta<2/3$ as a *crossover region*, where doping starts to build the Luttinger liquid, which is fully established for $\delta>2/3$.

We have also calculated the charge compressibility κ through

$$\chi=\frac{1}{n_0^2\kappa}=\frac{V}{4}[E(N_e+2)+E(N_e-2)-2E(N_e)], \tag{13}$$

where V is the volume and $n_0=\frac{N_e}{V}$ is the electronic density; the charge excitation velocity

$$u_\rho=\frac{E(\Delta k,S=0)-E_{\mathrm{GS}}}{\Delta k}, \tag{14}$$

with $\Delta k=2\pi/L$ and L the system length; and the Drude weight

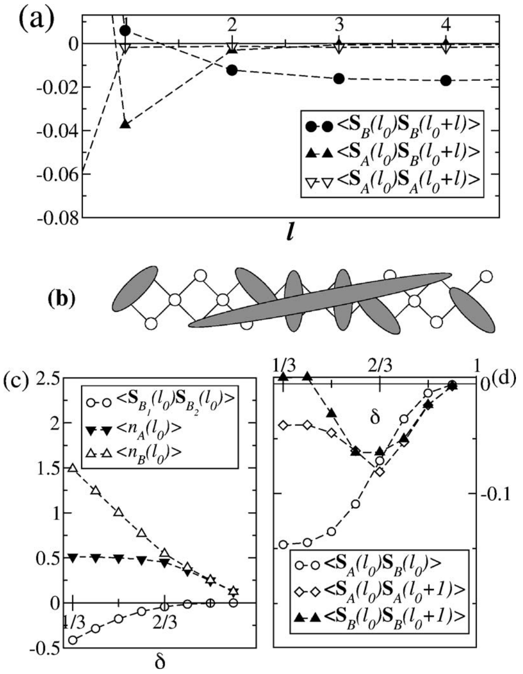

FIG. 9. (a) ED results for the indicated spin correlation functions as a function of cell index l, with $\mathbf{S}_B\equiv\mathbf{S}_{B_1}+\mathbf{S}_{B_2}$. (b) Illustration of the GS at $\delta=1/3$ doped with two holes: singlet bonds are represented by ellipses and holes by circles. (c) ED results for the spin correlation functions between B sites at the same cell $\langle \mathbf{S}_{B_1}(l_0)\cdot\mathbf{S}_{B_2}(l_0)\rangle$, electron densities at A sites $\langle n_A(l_0)\rangle$, and at $B\equiv B_1+B_2$ sites $\langle n_B(l_0)\rangle\equiv\langle n_{B_1}(l_0)+n_{B_2}(l_0)\rangle$. (d) ED results for the indicated nearest-neighbor spin correlation functions as a function of δ, with $\mathbf{S}_B\equiv\mathbf{S}_{B_1}+\mathbf{S}_{B_2}$. In (a), (c), and (d), l_0 denotes an arbitrary cell.

$$D=\frac{L}{4\pi}\left[\frac{\partial^2E(\Phi)}{\partial\Phi^2}\right]_{\Phi_{\min}}, \tag{15}$$

where $\Phi_{\min}$ is the flux value that minimizes the energy.[46] In an insulating phase, these quantities satisfy the limits below

$$\lim_{N_c\to\infty}\begin{cases}\chi=\infty\,,\\ u_\rho=\infty\,,\\ D=0,\end{cases} \tag{16}$$

while for a metal, χ, u_ρ, and D are finite. As shown in Fig. 10, at $\delta=1/3$, χ and u_ρ increase, while D decreases with system size for both $U=2$ and $U=\infty$, although the insulating character is better evidenced for $U=\infty$ due to its sizable charge gap, as shown in Fig. 7(a). At the other commensurate density, $\delta=2/3$, we can see the signals of an insulating phase for $U=\infty$, while for $U=2$ we do not observe any special behavior. In order to clarify this point, we have used DMRG to study the size dependence of the charge gap for larger systems at this doping. For a finite open chain, the occupation of two holes per cell tends to $\delta=2/3$ in the thermodynamic limit. In Fig. 11(a), we can clearly observe that for $U=\infty$ the system is in a Mott insulating phase with $\Delta_c\approx0.15$; however, the gap for $U=2$ is extremely small. In order to better understand the U dependence of this gap, we

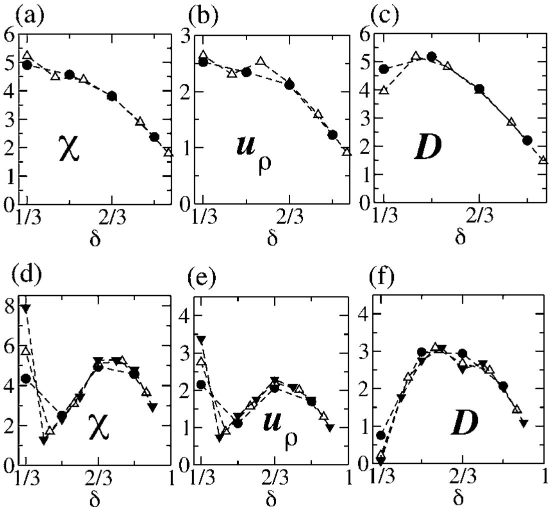

FIG. 10. ED results for the charge susceptibility χ, the charge excitation velocity u_ρ, and the Drude weight D, for $U=2$ [(a), (b), and (c)] and $U=\infty$ [(d), (e), and (f)], and $N_c=4$ (●), 6 (△), and 8 (▼).

have also calculated Δ_c for intermediate values of U, as also shown in Fig. 11(a). In the inset of Fig. 11(a), we have fit $\Delta_c(U)$ using an expression similar to the limiting behavior of the charge gap as $U\rightarrow 0$ of the Lieb-Wu solution for a linear chain at half-filling:[47] $U^a\exp(-b/x)$, in which $a\approx 0.61$ and $b\approx 7.95$ are fitting parameters. Notice, however, that contrary to the Lieb-Wu solution,[47] Δ_c saturates to a finite value (≈ 0.15) for $U=\infty$. On the other hand, similarly to the linear chain at half-filling,[47] the data shown in Fig. 11(b) indicate the absence of a spin gap at $\delta=2/3$ in the thermodynamic limit for both $U=2$ and $U=\infty$.

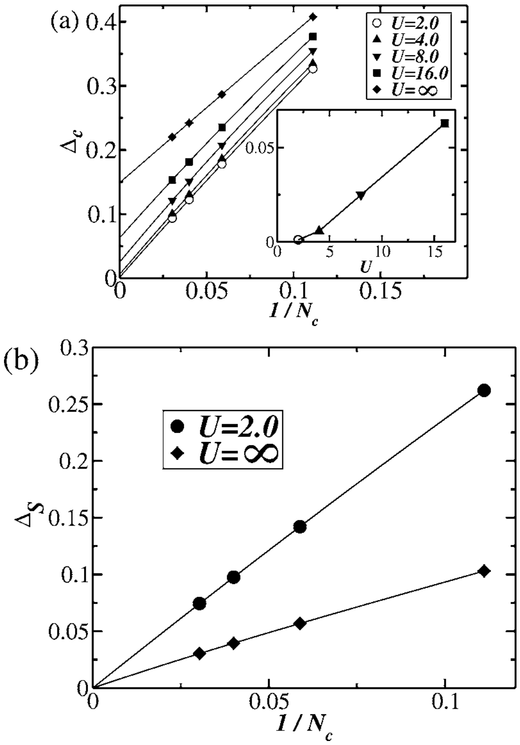

FIG. 11. DMRG results for (a) the charge gap Δ_c as a function of $1/N_c$ at $\delta=2/3$ using DMRG; the inset presents extrapolated values of the charge gap as a function of U. DMRG calculation of (b) the spin gap Δ_S as a function of $1/N_c$ for $U=2$ (●) and $U=\infty$ (◆). Solid lines are polynomial fittings, except in the inset of (a), where we have used an essential singularity form as explained in the text.

In the Luttinger model, it is well known[9] that χ, u_ρ, and D are related through

$$D=2u_\rho K_\rho \tag{17}$$

with

$$K_\rho=\frac{\pi u_\rho}{2\chi}, \tag{18}$$

where K_ρ is the exponent governing the decay of the correlation functions. In order to probe the doped region for which the lower-energy spectrum of the AB_2 chain can be mapped onto the Luttinger model, we consider the ratio

$$\frac{u_\rho}{\sqrt{D\chi/\pi}}, \tag{19}$$

which must be equal to 1 if the system is in the LL universality class.[48]

Since the AB_2 chain is not strictly one-dimensional, care must be taken with the length scales (V and L) in Eqs. (13)–(15). For $U=0$, the orbitals at sites A and bonding orbitals at sites B are translationally equivalent and both build the dispersive branches shown in Fig. 1(c). In this case, the system can be mapped onto a tight-binding linear chain with $2N_c$ sites and a rescaled hopping parameter, $t\rightarrow t\sqrt{2}$, with $K_\rho=1$. In order that Eq. (18) matches this result for $\epsilon_F<0$, we must choose $V\equiv L=2N_c$ with $\epsilon(k)=-2\sqrt{2}\cos(k)$, or, likewise, $V\equiv L=N_c$ and the dispersions as written in Eq. (3). In both cases $k_F=\frac{\pi}{2}n_0$, with $n_0=\frac{N_e}{L}$. Consider, for example, the former option. For $U=0$, the charge excitation velocity is equal to the Fermi velocity u_F, which can be easily calculated as

$$u_F=\left.\frac{\partial\epsilon(k)}{\partial k}\right|_{k=k_F}=2\sqrt{2}\sin(k_F). \tag{20}$$

On the other hand, substituting the GS energy,

$$E_{\mathrm{GS}}(n_0)=\frac{-8\sqrt{2}}{\pi}N_c\sin\left(\frac{\pi}{2}n_0\right), \tag{21}$$

into the continuous version of Eq. (13), we obtain

$$\chi=\frac{1}{V}\frac{\partial^2E_{\mathrm{GS}}}{\partial n_0^2} \tag{22}$$

$$=\pi\sqrt{2}\sin\left(\frac{\pi}{2}n_0\right). \tag{23}$$

Using now Eqs. (20) and (23) in Eq. (18), we find, as expected, $K_\rho=1$.

We now turn to the interacting case using ED. As shown in Fig. 12(a), the LL character is quite clear for $\delta>2/3$,

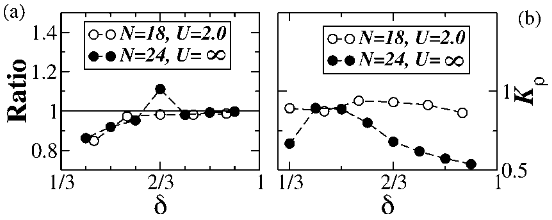

FIG. 12. (a) ED results for the ratio $u_\rho/\sqrt{D\chi/\pi}$. (b) ED results for K_ρ as a function of δ.

while for $1/3<\delta<2/3$ we identify the crossover region. The ED results for K_ρ are presented in Fig. 12(b). Notice that K_ρ is close to 1 (noninteracting fermions) for $U=2$, while K_ρ is close to 1/2 (noninteracting *spinless* fermions) for $U=\infty$.[9,49] In order to check these results, we used DMRG to calculate the ELC spin correlation function

$$C(l) \equiv \frac{\sum_{i,j} \langle \mathbf{S}_i \cdot \mathbf{S}_j \rangle \delta_{|i-j|,l}}{\sum_{i,j} \delta_{|i-j|,l}}, \tag{24}$$

whose asymptotic behavior should match that for the Luttinger model,[49]

$$C_{\mathrm{LL}}(l) \sim \frac{\cos(2k_F l)[\ln(l)]^{1/2}}{l^{1+K_\rho}}. \tag{25}$$

In Eq. (24), we have considered an average over all possible pairs of sites separated by the same distance l, a procedure that reduces open boundary effects. In Figs. 13(a) and 13(b), we show $C(l)$ calculated at $\delta=88/106$ for $U=2$ and $U=\infty$, respectively. Also shown are the fittings to $C(l)$ using $C_{\mathrm{LL}}(l)$ with $k_F=\frac{\pi}{2}n_0$ and K_ρ taken from the results shown in Fig. 12(b) after linear interpolation: $K_\rho=0.89$ ($U=2$) and $K_\rho=0.57$ ($U=\infty$). Motivated by a compromise between large values of l and minimum boundary effects, we have considered intermediate values of l in the fitting, which is quite good for both values of U. We thus conclude that the Luttinger model correctly describes the low-energy physics of the AB_2 chain for $\delta>2/3$.

VI. SUMMARY AND CONCLUSIONS

In summary, the numerical results presented here have clearly evidenced the rich phase diagram exhibited by the Hubbard model on the doped AB_2 chain both for $U=2$ and in the infinite-U limit. We have shown that at the commensurate dopings $\delta=1/3$ and $2/3$, the system displays insulating phases, although for $U=2$ the charge gap Δ_c is very small at $\delta=2/3$, with indications that Δ_c present an essential singularity as $U\to 0$. For $U=2$ and $\delta \lesssim 0.02$, the GS exhibit a ferrimagnetic phase reminiscent of the undoped regime, while for $0.02 \lesssim \delta \lesssim 0.07$, incommensurate magnetic correlations are observed. For $U=\infty$ and $\delta=0$, the GS total spin is degenerate, whereas for $0<\delta \lesssim 0.225$, hole itinerancy (Nagaoka mechanism) sets a fully polarized GS. In this case, we have also observed the presence of an extensive number of low-lying levels with total spin ranging from the minimum value to $S_{\max}-1$ and level spacing decaying with system size as $1/N_c$. For higher doping, the system phase-separates into coexisting metallic and insulating phases for $\delta_{\mathrm{PS}}(U) \lesssim \delta < 1/3$ [with $\delta_{\mathrm{PS}}(\infty) \approx 0.225$ and $\delta_{\mathrm{PS}}(2) \approx 0.07$]. The insulating state presents a finite spin gap and fully fills the system at $\delta=1/3$, which is well described by a short-ranged-RVB state. Finally, a crossover region is observed for $1/3<\delta<2/3$, while a Luttinger-liquid behavior is explicitly characterized for $\delta>2/3$.

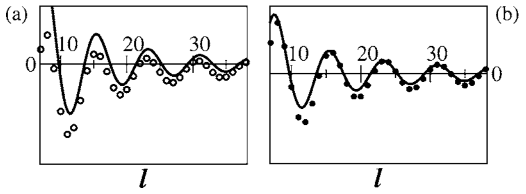

FIG. 13. Spin correlation functions $C(l)$ for (a) $U=2$ and (b) $U=\infty$ at $\delta=88/106$ for $N=106$ using DMRG: solid lines are fittings using Eq. (25).

In closing, we would like to stress that the above-reported results might also stimulate further experimental and theoretical investigations on quasi-one-dimensional compounds displaying complex unit-cell structures.[50]

ACKNOWLEDGMENTS

We acknowledge useful discussions with A. L. Malvezzi and M. H. Oliveira. This work was supported by CNPq, Finep, FACEPE, and CAPES (Brazilian agencies).

APPENDIX: VARIATIONAL APPROACH FOR $U=\infty$ AND $\delta \lesssim 1/3$

In the metallic saturated ferromagnetic region (parity symmetry −1), the energy as a function of doping is known to have a noninteracting spinless fermion behavior,

$$E(k_{F-}) = -\frac{4\sqrt{2}}{\pi} L_- \sin(k_{F-}/2), \tag{A1}$$

where $k_{F-}=\pi\nu_{h-}$, $\nu_{h-}=N_{h-}/L_-$, and L_- is the linear size of the system. On the other hand, in the insulating paramagnetic phase (SR-RVB states with even-parity symmetry) at $\delta=1/3$ (one hole per cell),

$$N_{h+} = L_+, \tag{A2}$$

and the energy per cell ϵ_+ is almost independent of the system linear size and can be estimated either by using ED or DMRG,

$$\epsilon_+ \approx -2.021. \tag{A3}$$

Let us now consider a phase-separated regime in which a paramagnetic phase with size L_+ coexists with a ferromagnetic one with size L_-, so the energy per cell reads

$$\epsilon = \epsilon_+ \frac{L_+}{N_c} - \frac{4\sqrt{2}}{\pi} \frac{L_-}{N_c} \sin\left(\frac{\pi}{2}\nu_{h-}\right). \tag{A4}$$

It is convenient to write ν_{h-} as

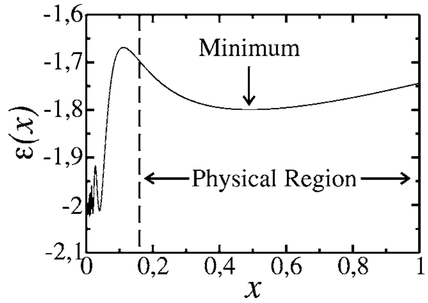

FIG. 14. Energy per unit cell ϵ as a function of the fraction $x=L_-/N_c$ for $\delta=0.28$. The physical region is also shown.

$$\nu_{h-}=\frac{N_h-(N_c-L_-)}{L_-}=\frac{3\delta-(1-x)}{x}, \qquad \text{(A5)}$$

where $N_h=N_{h+}+N_{h-}$, $N_c=L_++L_-$, $x=L_-/N_c$, and $N=3N_c$. Using the above notation, we rewrite Eq. (A4) in the form below,

$$\epsilon(x)=(1-x)\epsilon_+-\frac{4\sqrt{2}}{\pi}x\sin\left[\frac{\pi}{2}\left(\frac{3\delta-1}{x}+1\right)\right]. \qquad \text{(A6)}$$

Here we should notice the presence of a singularity at $x=0$ for any finite value of $\delta\neq 1/3$ (see Fig. 14). However, the region of physical values of x is defined by

$$0\leq N_{h+}\leq N_h, \qquad \text{(A7)}$$

i.e.,

$$1-3\delta\leq x\leq 1. \qquad \text{(A8)}$$

In Fig. 14, we present $\epsilon(x)$ for $\delta=0.28$, in which the physical region is $0.16\leq x\leq 1$ and can be found by Eq. (A8), with a minimum in $\epsilon(x)$ for $x\approx 0.49$.

The value of x that minimizes the energy for a given δ, $\bar{x}=\bar{x}(\delta)$, satisfies the equation $\left[\frac{\partial\epsilon(x)}{\partial x}\right]_\delta=0$, which can be written as

$$\frac{\pi\epsilon_+}{4\sqrt{2}}=\cos(y)+y\sin(y), \qquad \text{(A9)}$$

where

$$y\equiv\frac{\pi}{2}\frac{3\delta-1}{\bar{x}}. \qquad \text{(A10)}$$

The roots of Eq. (A9) are numerically calculated and conduct to

$$\bar{x}=1 \quad \text{for } \delta\lesssim 0.225,$$

$$\bar{x}\approx 3.071-9.213\delta \quad \text{for } 0.225\lesssim\delta\lesssim\frac{1}{3}. \qquad \text{(A11)}$$

We thus conclude that $\delta_{\text{PS}}(\infty)\approx 0.225$, which is in very good agreement with ED and DMRG calculations.

The magnetization is null at the even phase and maximum at the odd one. We can thus derive the following expression for the GS total spin per unit cell:

$$\frac{S_g}{N_c}=\frac{1}{2N_c}(N_e-2L_+) \qquad \text{(A12)}$$

$$=\frac{1}{2}[3(1-\delta)-2(1-\bar{x})]. \qquad \text{(A13)}$$

The dependence of the average parity p on δ can also be easily written as

$$p=1-2\bar{x}. \qquad \text{(A14)}$$

Finally, using Eq. (A11) for $\bar{x}$, the above results for p and S_g are plotted in Figs. 2(d) and 3(c), respectively, and shown to be in excellent agreement with the ED and DMRG calculations.

---

[1] P. W. Anderson, Science **235**, 1196 (1987).

[2] H. J. Schulz, Phys. Rev. Lett. **64**, 1445 (1990); B. M. Andersen and P. Hedegard, *ibid.* **95**, 037002 (2005).

[3] Y. Nagaoka, Phys. Rev. **147**, 392 (1966).

[4] H. Tasaki, Prog. Theor. Phys. **99**, 489 (1998) and references therein, including those describing the occurrence of flatband, or nearly flatband, saturated ferromagnetism at finite U.

[5] Saturated ferromagnetism in the square lattice was recently shown to occur in the infinite-U limit and a unit flux quantum per electron: Y. Saiga and M. Oshikawa, Phys. Rev. Lett. **96**, 036406 (2006).

[6] P. W. Anderson, *The Theory of Superconductivity in the High-T_c Cuprates* (Princeton University Press, Princeton, 1997).

[7] V. J. Emery, S. A. Kivelson, and H. Q. Lin, Phys. Rev. Lett. **64**, 475 (1990).

[8] E. Dagotto, Science **309**, 257 (2005).

[9] F. D. M. Haldane, J. Phys. C **14**, 2585 (1981); J. Voit, Rep. Prog. Phys. **58**, 977 (1995).

[10] A. M. S. Macêdo, M. C. dos Santos, M. D. Coutinho-Filho, and C. A. Macêdo, Phys. Rev. Lett. **74**, 1851 (1995).

[11] G. Sierra, M. A. Martín-Delgado, S. R. White, D. J. Scalapino, and J. Dukelsky, Phys. Rev. B **59**, 7973 (1999).

[12] Y. Watanabe and S. Miyashita, J. Phys. Soc. Jpn. **68**, 3086 (1999).

[13] M. A. Martín-Delgado, J. Rodriguez-Laguna, and G. Sierra, Phys. Rev. B **72**, 104435 (2005).

[14] G.-S. Tian and T.-H. Lin, Phys. Rev. B **53**, 8196 (1996).

[15] C. P. de Melo and S. A. F. Azevedo, Phys. Rev. B **53**, 16258 (1996).

[16] Y. F. Duan and K. L. Yao, Phys. Rev. B **63**, 134434 (2001); W. Z. Wang, Bambi Hu, and K. L. Yao, *ibid.* **66**, 085101 (2002).

[17] R. R. Montenegro-Filho and M. D. Coutinho-Filho, Physica A

357, 173 (2005).

[18] T. Nakanishi and S. Yamamoto, Phys. Rev. B **65**, 214418 (2002); C. Vitoriano, F. B. de Brito, E. P. Raposo, and M. D. Coutinho-Filho, Mol. Cryst. Liq. Cryst. Sci. Technol., Sect. A **374**, 185 (2002).

[19] F. C. Alcaraz and A. L. Malvezzi, J. Phys. A **30**, 767 (1997).

[20] E. P. Raposo and M. D. Coutinho-Filho, Phys. Rev. Lett. **78**, 4853 (1997); Phys. Rev. B **59**, 14384 (1999).

[21] M. H. Oliveira, M. D. Coutinho-Filho, and E. P. Raposo, Phys. Rev. B **72**, 214420 (2005).

[22] C. Vitoriano, M. D. Coutinho-Filho, and E. P. Raposo, J. Phys. A **35**, 9049 (2002).

[23] J. B. Anderson, E. Kostiner, and F. A. Ruszala, J. Solid State Chem. **39**, 29 (1981).

[24] M. Drillon, M. Belaiche, P. Legoll, J. Aride, A. Boukhari, and A. Moqine, J. Magn. Magn. Mater. **128**, 83 (1993).

[25] A. A. Belik, A. Matsuo, M. Azuma, K. Kindo, and M. Takano, J. Solid State Chem. **178**, 709 (2005).

[26] M. Matsuda, K. Kakurai, A. A. Belik, M. Azuma, M. Takano, and M. Fujita, Phys. Rev. B **71**, 144411 (2005).

[27] A. Boukhari, A. Moqine, and S. Flandrois, Mater. Res. Bull. **21**, 395 (1986).

[28] H. Effenberger, J. Solid State Chem. **142**, 6 (1999).

[29] M. Verdaguer, M. Julve, A. Michalowicz, and O. Kahn, Inorg. Chem. **22**, 2624 (1983); Y. Pei, M. Verdaguer, O. Kahn, J. Sletten, and J.-P. Renard, *ibid.* **26**, 138 (1987); P. J. van Koningsbruggen, O. Kahn, K. Nakatani, Y. Pei, J. P. Renard, M. Drillon, and P. Legoll, *ibid.* **29**, 3325 (1990).

[30] S. K. Pati, S. Ramasesha, and D. Sen, Phys. Rev. B **55**, 8894 (1997); S. Yamamoto, S. Brehmer, and H.-J. Mikeska, *ibid.* **57**, 13610 (1998); N. B. Ivanov, *ibid.* **62**, 3271 (2000); S. Yamamoto, *ibid.* **69**, 064426 (2004), and references therein.

[31] Y. Hosokoshi, K. Katoh, Y. Nakazawa, H. Nakano, and K. Inoue, J. Am. Chem. Soc. **123**, 7921 (2001); K. L. Yao, Q. M. Liu, and Z. L. Liu, Phys. Rev. B **70**, 224430 (2004); K. L. Yao, H. H. Fu, and Z. L. Liu, Solid State Commun. **135**, 197 (2005).

[32] S. A. Kivelson, I. P. Bindloss, E. Fradkin, V. Oganesyan, J. M. Tranquada, A. Kapitulnik, and C. Howald, Rev. Mod. Phys. **75**, 1201 (2003).

[33] E. H. Lieb, Phys. Rev. Lett. **62**, 1201 (1989).

[34] S. R. White, Phys. Rev. B **48**, 10345 (1993); U. Schollwöck, *ibid.* **77**, 259 (2005).

[35] R. Jullien and R. M. Martin, Phys. Rev. B **26**, 6173 (1982).

[36] A. A. Aligia and G. Ortiz, Phys. Rev. Lett. **82**, 2560 (1999); Raffaele Resta and Sandro Sorella, *ibid.* **82**, 370 (1999).

[37] S. Liang and H. Pang, Europhys. Lett. **32**, 173 (1995); M. Kohno, Phys. Rev. B **56**, 15015 (1997); H. Ueda and T. Idogaki, *ibid.* **69**, 104424 (2004).

[38] M. Troyer, H. Tsunetsugu, and T. M. Rice, Phys. Rev. B **53**, 251 (1996).

[39] F. Becca and S. Sorella, Phys. Rev. Lett. **86**, 3396 (2001).

[40] K. Kusakabe and H. Aoki, Phys. Rev. B **52**, R8684 (1995).

[41] T. Koma and H. Tasaki, J. Stat. Phys. **76**, 745 (1994); R. Arita and H. Aoki, Phys. Rev. B **61**, 12261 (2000).

[42] S. R. White and D. J. Scalapino, Phys. Rev. B **61**, 6320 (2000).

[43] E. Eisenberg, R. Berkovits, David A. Huse, and B. L. Altshuler, Phys. Rev. B **65**, 134437 (2002).

[44] D. S. Rokhsar and S. A. Kivelson, Phys. Rev. Lett. **61**, 2376 (1988).

[45] A. Giesekus, Phys. Rev. B **52**, 2476 (1995).

[46] R. M. Fye, M. J. Martins, D. J. Scalapino, J. Wagner, and W. Hanke, Phys. Rev. B **44**, 6909 (1991).

[47] E. H. Lieb and F. Y. Wu, Phys. Rev. Lett. **20**, 1445 (1968).

[48] See, e.g., C. A. Hayward and D. Poilblanc, Phys. Rev. B **53**, 11721 (1996).

[49] A. Parola and S. Sorella, Phys. Rev. Lett. **64**, 1831 (1990); H. J. Schulz, *ibid.* **64**, 2831 (1990).

[50] C. D. Batista and B. S. Shastry, Phys. Rev. Lett. **91**, 116401 (2003).